Advances in Aerodynamics

RESEARCH Open Access

A Gaussian process regression accelerated multiscale model for conduction-radiation heat transfer in periodic composite materials with temperature-dependent thermal properties

Zi-Xiang Tong[1], Ming-Jia Li[2*], Zhaolin Gu[1], Jun-Jie Yan[3] and Wen-Quan Tao[2]

*Correspondence:
mjli1990@mail.xjtu.edu.cn

[1] School of Human Settlements and Civil Engineering, Xi'an Jiaotong University, Xi'an 710049, Shaanxi, China
[2] Key Laboratory of Thermo-Fluid Science and Engineering of Ministry of Education, School of Energy and Power Engineering, Xi'an Jiaotong University, Xi'an 710049, Shaanxi, China
[3] School of Energy and Power Engineering, Xi'an Jiaotong University, Xi'an 710049, Shaanxi, China

Abstract

Prediction of the coupled conduction-radiation heat transfer in composite materials with periodic structure is important in high-temperature applications of the materials. The temperature dependence of thermal properties complicates the problem. In this work, a multiscale model is proposed for the conduction-radiation heat transfer in periodic composite materials with temperature-dependent thermal properties. Homogenization analysis of the coupled conduction and radiative transfer equations is conducted, in which the temperature dependence of thermal properties is considered. Both the macroscopic homogenized equations and the local unit cell problems are derived. It is proved that the macroscopic average temperature can be used in the unit cell problems for the first-order corrections of the temperature and radiative intensity, and the calculations of effective thermal properties. The temperature dependence of thermal properties only influences the higher-order corrections. A multiscale numerical method is proposed based on the analysis. The Gaussian process (GP) regression is coupled into the multiscale algorithm to build a correlation between thermal properties and temperature for the macroscale iterations and prevent the repetitive solving of unit cell problems. The GP model is updated by additional solutions of unit cell problems during the iteration according to a variance threshold. Numerical simulations of conduction-radiation heat transfer in composite with isotropic and anisotropic periodic structures are used to validate the proposed multiscale model. It is found that the accuracy and efficiency of the multiscale method can be guaranteed by using a proper variance threshold for the GP model. The multiscale model can provide both the average temperature and radiative intensity fields and their detailed fluctuations due to the local structures.

Keywords: Multiscale model, Heat Conduction, Radiative transfer equation, Temperature-dependent, Gaussian process regression, Machine learning

1 Introduction

Prediction of the heat transfer in composite materials with periodic structures is important in many applications, from the insulation of buildings to the thermal protection of space vehicles [1–3]. Among a variety of prediction methods, homogenization techniques combine both macroscopic and microscopic solutions and can provide multiscale results in periodic composites [4, 5]. The temperature field is divided into a macroscopic temperature field and local perturbations due to microscopic structures. The asymptotic analysis derives macroscopic governing equations for the whole material and governing equations in a representative unit cell. It also establishes the relation between macroscopic effective thermal properties and results of unit cell problems. The homogenization methods have been widely used in calculations of heat transfer in periodic composites [6–8], and are extended to the coupled conduction convection and radiation heat transfer problems [9–16]. The radiative transfer equation is also included in recent research [17].

In many works, the thermal properties of materials are assumed to be constant in the analysis. In practice, the thermal properties of real materials often depend on temperature. Therefore, the heat conduction in composite materials with temperature-dependent thermal conductivities is studied in some research. For example, Muliana and Kim [18] proposed a two-scale homogenization framework for laminated composites. The thermal conductivities of the components in the micromechanical model were temperature-dependent. Chung et al. [19] applied asymptotic expansion homogenization for composite materials with nonlinear properties. The thermal conductivities of the components in the unit cell problem were determined by the macroscopic average temperature or the non-uniform local temperature. Numerical tests demonstrated that the differences between the two approaches were insignificant. Zhai et al. [20] studied the transient heat conduction in composite materials with temperature-dependent thermal properties. The macroscopic average temperature was also used in the determination of the thermal properties in their unit cell problem. However, detailed asymptotic analysis of the heat conduction equation with temperature-dependent thermal properties is still needed.

Another problem associated with the multiscale model with temperature-dependent thermal properties is that the computational cost will be expensive. The effective thermal properties for the macroscopic model are provided by the solutions of the microscopic model. Because the temperature influences the thermal properties in the microscopic model, the microscopic model should be solved repetitively at each macroscopic iteration point, and the computational cost is unacceptable. This problem can be solved by reducing the order of the microscopic model [21]. For example, Monteiro et al. [22] used the proper orthogonal decomposition to reduce the order of the micro problem and simplify the computation. Another convenient approach is to build lists, fitted equations or surrogate models for the thermal properties to substitute the repetitive microscopic calculations. These surrogate models can be built before the macroscopic calculation based on preliminary microscopic calculations. They can be also built "on-the-fly", which means the surrogate models are updated during the calculations of macroscopic models [23, 24]. In recent years, the rapid developing artificial intelligence and machine learning models provide tools for

the multiscale methods. The machine learning models have been used in the hybrid atomistic-continuum simulations to substitute the microscopic molecular dynamics and complement the macroscopic continuum model [25, 26]. Stephenson et al. [27] employed the Gaussian process (GP) regression model in their hybrid model. The advantage of the GP model is that it estimates the errors of the predictions simultaneously [28]. A threshold of the error can be used to automatically indicate when the update of the GP model and the additional microscopic calculations are needed. Therefore, it is promising to combine the machine learning model with the homogenization model to improve its efficiency for problems with temperature-dependent thermal properties.

In this work, a homogenization method will be proposed for the coupled heat conduction and radiative transfer equations with temperature-dependent properties, and the GP regression model will be employed to accelerate the multiscale simulations. The rest of the paper is organized as follows. In Section 2, an asymptotic analysis will be conducted on the heat conduction equation and radiative transfer equation. The temperature dependence of the thermal properties will be considered in the analysis and a homogenization model will be established. In Section 3, the GP regression model will be introduced first. An accelerated multiscale algorithm based on the GP regression model will be proposed. Some numerical examples are used to validate the proposed multiscale model in Section 4. Finally, conclusions will be presented in Section 5.

2 Homogenization of conduction and radiative transfer equations

The coupled heat conduction equation and radiative transfer equation are as follows [29]:

$$\frac{\partial}{\partial x_i}\left(k_{ij}^{\varepsilon}\left(\mathbf{x}, T^{\varepsilon}\right)\frac{\partial T^{\varepsilon}(\mathbf{x})}{\partial x_j}\right) - \alpha^{\varepsilon}\left(\mathbf{x}, T^{\varepsilon}\right)\left(4\sigma_{\mathrm{B}}[T^{\varepsilon}(\mathbf{x})]^4 - \int_{4\pi} I^{\varepsilon}(\mathbf{x}, \Omega)\mathrm{d}\Omega\right) = 0, \tag{1}$$

$$\begin{aligned}\Omega_i\frac{\partial I^{\varepsilon}(\mathbf{x}, \Omega)}{\partial x_i} = &-\beta^{\varepsilon}\left(\mathbf{x}, T^{\varepsilon}\right)I^{\varepsilon}(\mathbf{x}, \Omega) + \frac{\sigma_{\mathrm{B}}}{\pi}\alpha^{\varepsilon}\left(\mathbf{x}, T^{\varepsilon}\right)[T^{\varepsilon}(\mathbf{x})]^4 \\ &+\frac{\sigma^{\varepsilon}(\mathbf{x}, T^{\varepsilon})}{4\pi}\int_{4\pi} I^{\varepsilon}\left(\mathbf{x}, \Omega'\right)\Phi^{\varepsilon}\left(\mathbf{x}, \Omega', \Omega\right)\mathrm{d}\Omega',\end{aligned} \tag{2}$$

where $\mathbf{x}=(x_1, x_2, x_3)$ is the coordinate and $\Omega=(\Omega_1, \Omega_2, \Omega_3)$ is the direction of the radiative intensity. The T^{ϵ} and I^{ε} are the temperature and the radiative intensity. The heat conductivity k_{ij}^{ε}, the extinction coefficient β^{ε}, the absorption coefficient α^{ε} and the scattering coefficient σ^{ε} are all functions of the coordinate and the temperature. The σ_{B} is the Stefan-Boltzmann constant. The Einstein summation convention is used in this paper, and the repetitive indices i and j imply summations over all the components.

The homogenization of the Eqs. (1) and (2) is similar to the analysis in Ref. [17]. A local coordinate $\mathbf{y}=\mathbf{x}/\varepsilon$ in a unit cell is introduced, as shown in Fig. 1. The ε can be regarded as the ratio between the characteristic length of the unit cell and the characteristic length of the whole material or computational domain. Therefore, ε is a small parameter when the material contains a large number of unit cells.

Then, the temperature and the radiative intensity are expanded as:

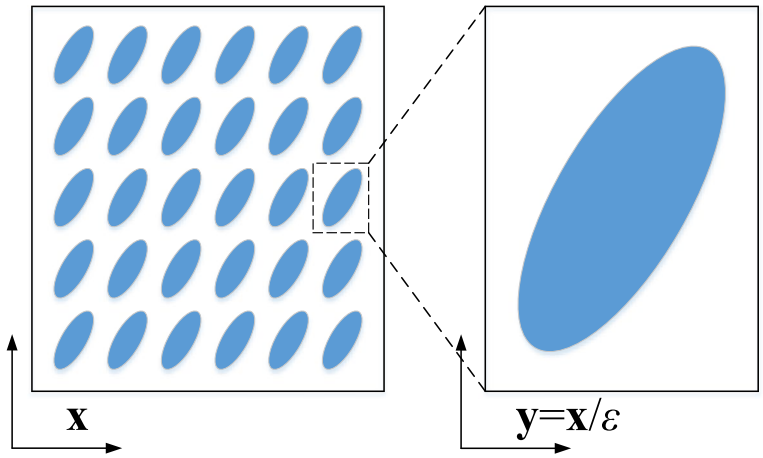

Fig. 1 Sketch of the computational domain for homogenization analysis

$$T^{\varepsilon}(\mathbf{x}) = T_0(\mathbf{x},\mathbf{y}) + \varepsilon T_1(\mathbf{x},\mathbf{y}) + \varepsilon^2 T_2(\mathbf{x},\mathbf{y}) + O\left(\varepsilon^3\right), \tag{3}$$

$$I^{\varepsilon}(\mathbf{x},\Omega) = I_0(\mathbf{x},\mathbf{y},\Omega) + \varepsilon I_1(\mathbf{x},\mathbf{y},\Omega) + O\left(\varepsilon^2\right), \tag{4}$$

where the T_1 and T_2 are periodic functions in a unit cell. It is also assumed that the volumetric averages of T_1, T_2 and I_1 in a unit cell are zero. The spatial derivative becomes:

$$\frac{\partial}{\partial x_i} \to \frac{\partial}{\partial x_i} + \frac{1}{\varepsilon}\frac{\partial}{\partial y_i}. \tag{5}$$

The thermal properties k_{ij}^{ε}, α^{ε}, β^{ε} and σ^{ε} are functions of both $\mathbf{y}$ and T^{ϵ}. In the present work, the Taylor expansions are used and the thermal properties are expressed as:

$$\varphi^{\varepsilon}\left(\mathbf{y},T^{\varepsilon}\right) = \varphi^{\varepsilon}\left(\mathbf{y},T_0\right) + \varepsilon T_1(\mathbf{x},\mathbf{y})\frac{\partial \varphi^{\varepsilon}\left(\mathbf{y},T_0\right)}{\partial T} + O\left(\varepsilon^2\right), \tag{6}$$

where ϕ represents any of the physical properties.

The Eqs. (3)-(6) are then submitted into Eqs. (1)-(2) to obtain the equations in different orders of ε. The detailed analysis can be found in Ref. [17], and the difference is that more terms are introduced into the equations by Eq. (6). However, it will be demonstrated that the temperature-dependent properties do not influence the macroscopic average equations and the first-order corrections.

The equation in the order of ε^{-2} still provides:

$$T_0 = T_0(\mathbf{x}). \tag{7}$$

The heat conduction equation in the order of ε^{-1} becomes:

$$\frac{\partial}{\partial x_i}\left(k_{ij}^{\varepsilon}(\mathbf{y},T_0)\frac{\partial T_0}{\partial y_j}\right) + \frac{\partial}{\partial y_i}\left[k_{ij}^{\varepsilon}(\mathbf{y},T_0)\frac{\partial T_0}{\partial x_j} + k_{ij}^{\varepsilon}(\mathbf{y},T_0)\frac{\partial T_1}{\partial y_j}\right] + \frac{\partial}{\partial y_i}\left[\left(T_1\frac{\partial k_{ij}^{\varepsilon}(\mathbf{y},T_0)}{\partial T}\right)\frac{\partial T_0}{\partial y_j}\right] = 0, \tag{8}$$

where the last term on the left-hand side is related to the variable thermal conductivity. Because $\partial T_0/\partial y_j = 0$, the first and last terms on the left-hand side can be eliminated. Therefore, the equation for unit cell problem is the same as that for problems with constant thermal properties, which is [17]:

$$\frac{\partial}{\partial y_i}\left(k_{ij}^{\varepsilon}(\mathbf{y},T_0)\frac{\partial N_\alpha(\mathbf{y},T_0)}{\partial y_j}\right) = -\frac{\partial k_{i\alpha}^{\varepsilon}(\mathbf{y},T_0)}{\partial y_i}, \tag{9}$$

with the following form of T_1:

$$T_1(\mathbf{x},\mathbf{y}) = N_\alpha(\mathbf{y},T_0)\frac{\partial T_0(\mathbf{x})}{\partial x_\alpha}. \tag{10}$$

The periodic boundary condition is still used for N_α and the volumetric average of N_α in a unit cell should be zero. Eq. (9) demonstrates that the thermal conductivity in the unit cell problem is determined by the macroscopic average temperature T_0. This analysis is also justified by the simulations in Ref. [19, 20], where the T_0 is used in the unit cell problems because of its simplicity.

As for the radiative transfer equation, the ε^{-1} order equation still provides:

$$I_0 = I_0(\mathbf{x},\Omega). \tag{11}$$

In the order of ε^0, the heat conduction equation gives:

$$\begin{aligned}&\frac{\partial}{\partial x_i}\left[k_{ij}^{\varepsilon}(\mathbf{y},T_0)\frac{\partial T_0}{\partial x_j}\right] + \frac{\partial}{\partial x_i}\left[k_{ij}^{\varepsilon}(\mathbf{y},T_0)\frac{\partial T_1}{\partial y_j}\right] + \frac{\partial}{\partial y_i}\left[k_{ij}^{\varepsilon}(\mathbf{y},T_0)\frac{\partial T_1}{\partial x_j}\right] + \frac{\partial}{\partial y_i}\left[k_{ij}^{\varepsilon}(\mathbf{y},T_0)\frac{\partial T_2}{\partial y_j}\right]\\ &+\frac{\partial}{\partial y_i}\left[\left(T_1\frac{\partial k_{ij}^{\varepsilon}}{\partial T}\right)\left(\frac{\partial T_0}{\partial x_j}+\frac{\partial T_1}{\partial y_j}\right)\right] = 4\alpha^{\varepsilon}(\mathbf{y},T_0)\sigma_{\mathrm{B}}T_0^4 - \alpha^{\varepsilon}(\mathbf{y},T_0)\int_{4\pi} I_0\mathrm{d}\Omega.\end{aligned} \tag{12}$$

Here $\partial T_0/\partial y_j = 0$ is already applied to eliminate a vanished term. The last term on the left-hand side is the additional term due to the thermal conductivity. The homogenized macroscopic equation is derived by integrating Eq. (12) in a unit cell. Because of the periodic properties of the variables in the unit cell, the terms started with $\partial[]/\partial y_i$ will be eliminated.

Therefore, the temperature-dependent thermal properties still have no influence on the macroscopic heat conduction equation, and the homogenized equation is:

$$\frac{\partial}{\partial x_i}\left[K_{ij}(T_0)\frac{\partial T_0}{\partial x_j}\right] - 4\overline{\alpha(T_0)}\sigma_{\mathrm{B}}T_0^4 + \overline{\alpha(T_0)}\int_{4\pi} I_0\mathrm{d}\Omega = 0. \tag{13}$$

The effective thermal conductivity K_{ij} is given by:

$$K_{ij}(T_0) = \frac{1}{|Y|}\int\left[k_{ij}^{\varepsilon}(\mathbf{y},T_0) + k_{i\alpha}^{\varepsilon}(\mathbf{y},T_0)\frac{\partial N_j(\mathbf{y},T_0)}{\partial y_\alpha}\right]\mathrm{d}\mathbf{y}, \tag{14}$$

where $|Y|$ is the volume of the unit cell, and the volumetric average value of a variable ϕ is defined as:

$$\overline{\varphi(T_0)} = \frac{1}{|Y|}\int \varphi(\mathbf{y}, T_0)\mathrm{d}\mathbf{y}. \tag{15}$$

The equations are the same as the equations derived with the constant thermal properties [17]. Therefore, the analysis further demonstrates that the macroscopic average temperature can be used in the unit cell problem to calculate the effective thermal properties.

However, the equations for the calculation of T_2 are more complex because of the additional terms and the dependence of T_0 on $\mathbf{x}$. The spatial derivatives of k_{ij}^{ε} and N_β are:

$$\frac{\partial k_{ij}^{\varepsilon}}{\partial x_\alpha} = \frac{\partial k_{ij}^{\varepsilon}}{\partial T}\frac{\partial T_0}{\partial x_\alpha}, \frac{\partial N_\beta}{\partial x_\alpha} = \frac{\partial N_\beta}{\partial T}\frac{\partial T_0}{\partial x_\alpha}. \tag{16}$$

Then, Eq. (12) can be reformed into:

$$\begin{aligned}&\left[k_{\alpha\beta}^{\varepsilon} + k_{\alpha i}^{\varepsilon}\frac{\partial N_\beta}{\partial y_i} + \frac{\partial\left(k_{\alpha i}^{\varepsilon}N_\beta\right)}{\partial y_i}\right]\frac{\partial^2 T_0}{\partial x_\alpha \partial x_\beta} + \left[\frac{\partial k_{\alpha\beta}^{\varepsilon}}{\partial T} + \frac{\partial}{\partial T}\left(k_{\alpha i}^{\varepsilon}\frac{\partial N_\beta}{\partial y_i}\right) + \frac{\partial}{\partial y_i}\left(k_{\alpha i}^{\varepsilon}\frac{\partial N_\beta}{\partial T}\right)\right]\frac{\partial T_0}{\partial x_\alpha}\frac{\partial T_0}{\partial x_\beta}\\ &+\frac{\partial}{\partial y_i}\left[\left(N_\beta\frac{\partial k_{ij}^{\varepsilon}}{\partial T}\right)\left(\delta_{\alpha j} + \frac{\partial N_\alpha}{\partial y_j}\right)\right]\frac{\partial T_0}{\partial x_\alpha}\frac{\partial T_0}{\partial x_\beta} + \frac{\partial}{\partial y_i}\left[k_{ij}^{\varepsilon}\frac{\partial T_2}{\partial y_j}\right] = 4\alpha^{\varepsilon}\sigma_{\mathrm{B}}T_0^4 - \alpha^{\varepsilon}\int_{4\pi} I_0\mathrm{d}\Omega,\end{aligned} \tag{17}$$

where all the properties are determined at T_0. Equation (13) can be also rewritten as:

$$K_{\alpha\beta}\frac{\partial^2 T_0}{\partial x_\alpha \partial x_\beta} + \frac{\partial K_{\alpha\beta}}{\partial T}\frac{\partial T_0}{\partial x_\alpha}\frac{\partial T_0}{\partial x_\beta} = 4\overline{\alpha(T_0)}\sigma_{\mathrm{B}}T_0^4 - \overline{\alpha(T_0)}\int_{4\pi} I_0\mathrm{d}\Omega. \tag{18}$$

The unit cell problems related to T_2 are derived by subtracting Eq. (18) from Eq. (17). According to the form of Eq. (17), the following ansatz for T_2 can be used:

$$T_2 = M_{\alpha\beta}(\mathbf{y}, T_0)\frac{\partial^2 T_0}{\partial x_\alpha \partial x_\beta} + P_{\alpha\beta}(\mathbf{y}, T_0)\frac{\partial T_0}{\partial x_\alpha}\frac{\partial T_0}{\partial x_\beta} + C(\mathbf{y}, T_0)\left(4\sigma_{\mathrm{B}}T_0^4 - \int_{4\pi} I_0\mathrm{d}\Omega\right). \tag{19}$$

The corresponding governing equations for the $M_{\alpha\beta}$, $P_{\alpha\beta}$ and C are:

$$\frac{\partial}{\partial y_i}\left(k_{ij}^{\varepsilon}\frac{\partial M_{\alpha\beta}}{\partial y_j}\right) = -\left[k_{\alpha\beta}^{\varepsilon} - K_{\alpha\beta} + k_{\alpha i}^{\varepsilon}\frac{\partial N_\beta}{\partial y_i} + \frac{\partial\left(k_{\alpha i}^{\varepsilon}N_\beta\right)}{\partial y_i}\right], \tag{20}$$

$$\frac{\partial}{\partial y_i}\left(k_{ij}^{\varepsilon}\frac{\partial P_{\alpha\beta}}{\partial y_j}\right) = -\left[\frac{\partial k_{\alpha\beta}^{\varepsilon}}{\partial T} + \frac{\partial}{\partial T}\left(k_{\alpha i}^{\varepsilon}\frac{\partial N_\beta}{\partial y_i}\right) - \frac{\partial K_{\alpha\beta}}{\partial T}\right] - \frac{\partial}{\partial y_i}\left[\frac{\partial\left(k_{\alpha i}^{\varepsilon}N_\beta\right)}{\partial T} + N_\beta\frac{\partial k_{ij}^{\varepsilon}}{\partial T}\frac{\partial N_\alpha}{\partial y_j}\right], \tag{21}$$

$$\frac{\partial}{\partial y_i}\left(k_{ij}^{\varepsilon}\frac{\partial C}{\partial y_j}\right) = \alpha^{\varepsilon} - \overline{\alpha}. \tag{22}$$

Compared with the analysis for problems with constant thermal properties in Ref. [17], it can be found that the equations for $M_{\alpha\beta}$ and C are the same, and the $P_{\alpha\beta}$ is the additional functions that should be solved. It is also easy to prove that the integrals of the right-hand sides of Eqs. (20)-(22) are all zero according to the periodic property of k_{ij}^{ε}

and N_α in a unit cell and the definition of $K_{\alpha\beta}$ in Eq. (14). The periodic boundary conditions can be still used for $M_{\alpha\beta}$, $P_{\alpha\beta}$ and C in a unit cell.

The previous research shows that the influence of T_2 on the accuracy of the temperature field is insignificant [17]. Because the present work mainly focuses on the computation of multiscale heat transfer problems with temperature-dependent thermal conductivities, the solution of T_2 is not considered and only T_0 and T_1 are calculated in this work for the temperature.

Finally, because the partial derivatives of thermal properties of the Eq. (6) are in the order of ε, they have no influence on the radiative transfer equations in the order of ε^{-1} and ε^0. Therefore, the equations for I_0 and I_1 are the same as those in Ref. [17]:

$$\Omega_i \frac{\partial I_0}{\partial x_i} = -\overline{\beta(T_0)} I_0 + \frac{\overline{\alpha(T_0)}\sigma_B}{\pi} T_0^4 + \frac{1}{4\pi}\int_{4\pi} I_0(\mathbf{x},\Omega')\overline{\sigma(T_0)\Phi(\Omega',\Omega)}\mathrm{d}\Omega', \tag{23}$$

$$\begin{aligned}\Omega_i \frac{\partial I_1}{\partial y_i} = &-\left(\beta^\varepsilon(T_0) - \overline{\beta(T_0)}\right) I_0 + \frac{\left(\alpha^\varepsilon(T_0) - \overline{\alpha(T_0)}\right)\sigma_B}{\pi} T_0^4 \\ &+ \frac{1}{4\pi}\int_{4\pi} I_0(\mathbf{x},\Omega')\left(\sigma^\varepsilon(T_0)\Phi^\varepsilon(T_0) - \overline{\sigma(T_0)\Phi}\right)\mathrm{d}\Omega'.\end{aligned} \tag{24}$$

It should be mentioned that a variety of boundary conditions of I_1 can be used for Eq. (24) in a unit cell. In the previous work, it is found that the periodic boundary condition will overpredict the fluctuations in the unit cell and lead to large errors [17]. It is suggested that the I_1 is solved in the whole region with the following boundary condition:

I_1 ($I_{1,\mathrm{all}}$) is solved in the whole domain with

$$I_1(\mathbf{x},\Omega) = 0, \text{ for } \Omega\cdot\mathbf{n} < 0, \mathbf{x}\in\Gamma, \tag{25}$$

where $\mathbf{n}$ is the outward unit normal and Γ is the boundary of the whole domain. The I_1 solved by Eq. (25) is denoted by $I_{1,\mathrm{all}}$ in this work. However, this treatment of I_1 still has two drawbacks. Firstly, the error of the radiation tends to accumulate from the incoming boundary to the outgoing boundary, and the fluctuations will be amplified. Secondly, it is inconvenient to obtain a local radiation fluctuation by solving I_1 in the entire region.

In this work, the following I_1 solved in an individual unit cell is used:

I_1 ($I_{1,\mathrm{cell}}$) is solved in an individual unit cell with

$$I_1(\mathbf{x},\Omega) = 0, \text{ for } \Omega\cdot\mathbf{n} < 0, \mathbf{x}\in\Gamma_Y, \tag{26}$$

where Γ_Y is the boundary of a unit cell. The I_1 solved by Eq. (26) is denoted by $I_{1,\mathrm{cell}}$ in this work. The boundary condition in Eq. (26) means that the incoming I_1 is zero in each unit cell, which is different from the periodic boundary condition. It is found that $I_{1,\mathrm{cell}}$ tends to underpredict the fluctuations. Therefore, the average of $I_{1,\mathrm{all}}$ and $I_{1,\mathrm{cell}}$ is also used as a boundary condition, which is calculated by:

$$I_{1,\mathrm{ave}} = \left(I_{1,\mathrm{all}} + I_{1,\mathrm{cell}}\right)/2. \tag{27}$$

In summary, the influence of the temperature-dependent thermal properties only appears in the equations for T_2. The macroscopic homogenized equations for T_0 and I_0 and the unit cell problems for T_1 and I_1 are the same as the equations for problems with

constant thermal properties. The macroscopic average temperature T_0 is used in these equations to determine the thermal properties. All the governing equations are summarized in Table 1 for convenience.

3 Gaussian process regression accelerated multiscale algorithm

According to the analysis in Section 2, a multiscale computational procedure can be proposed for the conduction-radiation heat transfer in periodic composite materials. A mesh for the macroscopic simulations and a mesh for the unit cell problems are firstly established. Then, the Eqs. (13) and (23) are solved to obtain the macroscopic T_0 and I_0. The effective thermal conductivities and radiative transfer coefficients are calculated from the solutions of the unit cell problems. Because the properties in the unit cell problems depend on the temperature, the above calculations of the effective properties should be employed in each iteration on all the mesh nodes. This procedure is unacceptable because the repetitive calculations of the unit cell problems under different temperatures will consume large computational resources.

Therefore, in the present work, the Gaussian process regression will be used as the surrogate model to obtain the correlation between the effective thermal conductivity and the temperature. In the rest of this section, the GP regression will be briefly introduced in Section 3.1, and the multiscale computational procedure will be described in Section 3.2.

3.1 Gaussian process regression

Details of the GP regression model can be found in Ref. [27, 28], and only the essential algorithms are described in this section. It is assumed that n thermal conductivity tensors $K_{ij,k}$, $k=1\sim n$, have been calculated from the unit cell problem before the regression, which are corresponding to the temperatures T_k. The vectors $\mathbf{K}_{ij}$ and $\mathbf{T}$ are defined as

Table 1 The summary of the equations for the homogenization of conduction and radiative transfer equations

Variables	Governing equations
T^ε	$T^\varepsilon(\mathbf{x}) = T_0(\mathbf{x},\mathbf{y}) + \varepsilon T_1(\mathbf{x},\mathbf{y},T_0) + \varepsilon^2 T_2(\mathbf{x},\mathbf{y},T_0)$
T_0	$\frac{\partial}{\partial x_i}\left[K_{ij}(T_0)\frac{\partial T_0}{\partial x_j}\right] - 4\overline{\alpha(T_0)}\sigma_B T_0^4 + \overline{\alpha(T_0)}\int_{4\pi} I_0 \mathrm{d}\Omega = 0,$
	$K_{ij} = \frac{1}{\lvert Y\rvert}\int\left[k_{ij}^\varepsilon(\mathbf{y},T_0) + k_{i\alpha}^\varepsilon(\mathbf{y},T_0)\frac{\partial N_j(\mathbf{y},T_0)}{\partial y_\alpha}\right]\mathrm{d}\mathbf{y}$
T_1	$T_1(\mathbf{x},\mathbf{y},T_0) = N_i(\mathbf{y},T_0)\frac{\partial T_0(\mathbf{x})}{\partial x_i}$
N_α	$\frac{\partial}{\partial y_i}\left(k_{ij}^\varepsilon(\mathbf{y},T_0)\frac{\partial N_\alpha(\mathbf{y},T_0)}{\partial y_j}\right) = -\frac{\partial k_{i\alpha}^\varepsilon(\mathbf{y},T_0)}{\partial y_i}$
T_2	$T_2 = M_{\alpha\beta}(\mathbf{y},T_0)\frac{\partial^2 T_0}{\partial x_\alpha \partial x_\beta} + P_{\alpha\beta}(\mathbf{y},T_0)\frac{\partial T_0}{\partial x_\alpha}\frac{\partial T_0}{\partial x_\beta} + C(\mathbf{y},T_0)\left(4\sigma_B T_0^4 - \int_{4\pi} I_0 \mathrm{d}\Omega\right)$
$M_{\alpha\beta}$	$\frac{\partial}{\partial y_i}\left(k_{ij}^\varepsilon\frac{\partial M_{\alpha\beta}}{\partial y_j}\right) = -\left[k_{\alpha\beta}^\varepsilon - K_{\alpha\beta} + k_{\alpha i}^\varepsilon\frac{\partial N_\beta}{\partial y_i} + \frac{\partial\left(k_{\alpha i}^\varepsilon N_\beta\right)}{\partial y_i}\right]$
$P_{\alpha\beta}$	$\frac{\partial}{\partial y_i}\left(k_{ij}^\varepsilon\frac{\partial P_{\alpha\beta}}{\partial y_j}\right) = -\left[\frac{\partial k_{\alpha\beta}^\varepsilon}{\partial T} + \frac{\partial}{\partial T}\left(k_{\alpha i}^\varepsilon\frac{\partial N_\beta}{\partial y_i}\right) - \frac{\partial K_{\alpha\beta}}{\partial T}\right] - \frac{\partial}{\partial y_i}\left[\frac{\partial\left(k_{\alpha i}^\varepsilon N_\beta\right)}{\partial T} + N_\beta\frac{\partial k_{ij}^\varepsilon}{\partial T}\frac{\partial N_\alpha}{\partial y_j}\right]$
C	$\frac{\partial}{\partial y_i}\left(k_{ij}^\varepsilon\frac{\partial C}{\partial y_j}\right) = \alpha^\varepsilon - \overline{\alpha}$
I^ε	$I^\varepsilon(\mathbf{x},\Omega) = I_0(\mathbf{x},\mathbf{y},\Omega) + \varepsilon I_1(\mathbf{x},\mathbf{y},\Omega)$
I_0	$\Omega_i\frac{\partial I_0}{\partial x_i} = -\overline{\beta(T_0)}I_0 + \frac{\overline{\alpha(T_0)}\sigma_B}{\pi}T_0^4 + \frac{1}{4\pi}\int_{4\pi} I_0(\mathbf{x},\Omega')\overline{\sigma(T_0)\Phi}(\Omega',\Omega)\mathrm{d}\Omega',$
	$\overline{\varphi(T_0)} = \frac{1}{\lvert Y\rvert}\int\varphi(\mathbf{y},T_0)\mathrm{d}y,\ \varphi$ is α, β or $\sigma\Phi$
I_1	$\Omega_i\frac{\partial I_1}{\partial y_i} = -\left(\beta^\varepsilon(T_0) - \overline{\beta(T_0)}\right)I_0 + \frac{\left(\alpha^\varepsilon(T_0) - \overline{\alpha(T_0)}\right)\sigma_B}{\pi}T_0^4 + \frac{1}{4\pi}\int_{4\pi} I_0(\mathbf{x},\Omega')\left(\sigma^\varepsilon(T_0)\Phi^\varepsilon(T_0) - \overline{\sigma(T_0)\Phi}\right)\mathrm{d}\Omega'$

$\mathbf{K}_{ij} = (K_{ij,1}, K_{ij,2}, \ldots, K_{ij,n})^{\mathrm{T}}$ and $\mathbf{T} = (T_1, T_2, \ldots, T_n)^{\mathrm{T}}$. In the GP model, the prior mean function is chosen as zero. The variance of the noise of $\mathbf{K}_{ij}$ is denoted by σ_n^2. The σ_n is chosen as the residual of the N_α, which is 10^{-7} in this work. The squared exponential covariance function is used in this paper:

$$C(T_i, T_j) = \sigma_f^2 \exp\left[-\frac{(T_i - T_j)^2}{2l^2}\right], \tag{28}$$

where σ_f and l are two hyperparameters. Then, the probability distribution of K_{ij}^* at temperature T^* is a Gaussian distribution with mean value [28]:

$$\overline{K}_{ij}^* = \mathbf{C}^*(T^*, \mathbf{T})^{\mathrm{T}}\left[\mathbf{C}(\mathbf{T}, \mathbf{T}) + \sigma_n^2\mathbf{I}\right]^{-1}\mathbf{K}_{ij}, \tag{29}$$

and the variance:

$$\sigma_*^2 = C(T^*, T^*) - \mathbf{C}^*(T^*, \mathbf{T})^{\mathrm{T}}\left[\mathbf{C}(\mathbf{T}, \mathbf{T}) + \sigma_n^2\mathbf{I}\right]^{-1}\mathbf{C}^*(T^*, \mathbf{T}), \tag{30}$$

where $\mathbf{C}^*$ is an $n \times 1$ vector with entries $C_k^* = C(T^*, T_k)$ and $\mathbf{C}$ is an $n \times n$ matrix with entries $C_{km} = C(T_k, T_m)$.

During the simulation, when the $\mathbf{C}$ and $\mathbf{K}_{ij}$ are calculated based on the existing data, the K_{ij}^* at a new temperature T^* can be predicted by Eq. (29). A variance σ_*^2 is also given by Eq. (30). If the σ_* exceeds a threshold σ_t which is specified before the simulation, a new unit cell problem of N_α will be called to calculate the K_{ij} at the new temperature. The new data will be added to the existing data set and the $\mathbf{C}$ and $\mathbf{K}_{ij}$ are updated. In addition, the σ_* is not relevant to $\mathbf{K}_{ij}$, as demonstrated by Eq. (30). Therefore, the threshold is the same for all the components of thermal conductivity tensor.

In practice, the two hyperparameters in the GP model need to be determined. A possible method is to use the maximum likelihood estimation (MLE) as mentioned in Ref. [27]. In the present work, we simply choose $l = T_h\text{-}T_c$ and $\sigma_f = 1$. The reason can be explained by the following test. The data is the K_{12} calculated from a unit cell with elliptical particle with temperature changing from 400 to 1400 K. The K_{12} for 400 K, 800 K, 1200 K and 1400 K are used to train a GP model. The MLE gives an optimized set of (σ_f, l) as (0.0075, 370.6). However, the K_{12} predicted with the optimized hyperparameters have large deviations compared with the real data, as shown in Fig. 2. On the contrary, the GP model with (σ_f, l) = (1, 1000) coincides better with the calculated data. The reason is that although the optimized hyperparameters by MLE are more consistent with the training data, the training data could not reflect the trend of the real data. It should be mentioned that although different hyperparameters provide different predictions, the parameter that controls the accuracy of the multiscale simulation is the threshold σ_t. In the present work, the (σ_f, l) = (1, 400) is used and the influence of σ_t will be discussed.

3.2 Multiscale computational procedure

The computational procedure for multiscale simulation with GP regression is given in Fig. 3. The procedure contains the following steps.

(1) Build meshes and initialize the macroscopic problems and the unit cell problems.

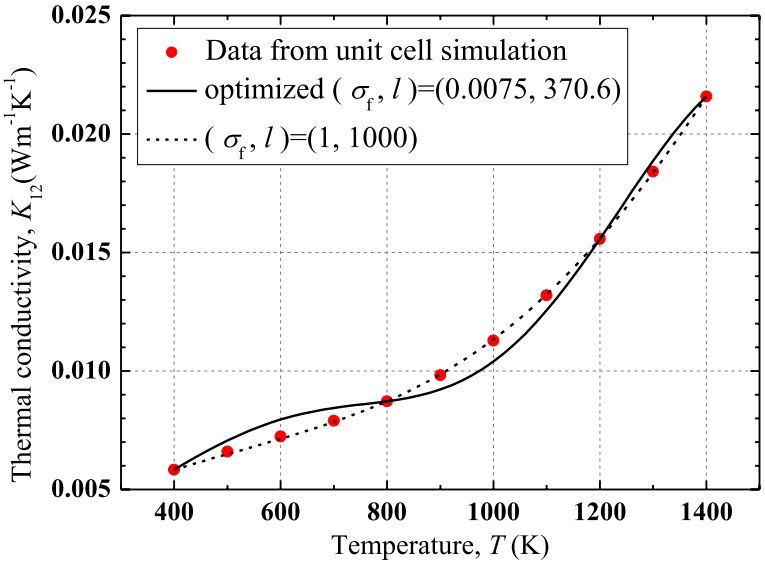

Fig. 2 Gaussian process regression model with different (σ_f, l) hyperparameters

(2) Select a set of initial temperatures. Solve Eq. (9) for N_α in the unit cell and calculate the effective thermal conductivity and radiative coefficients by Eqs. (14) and (15).
(3) Build an initial GP model for the thermal properties by calculating the matrix $\left[\mathbf{C}(\mathbf{T},\mathbf{T})+\sigma_n^2\mathbf{I}\right]^{-1}$ in Eqs. (29) and (30).
(4) The macroscopic homogenized Eqs. (13) and (23) are iterated, while the thermal properties are calculated from the GP model. Equation (30) is firstly used to obtain the σ_* according to the current temperature of the grid node. If σ_* is smaller than the threshold σ_t, Eq. (29) is used to calculate the thermal properties. Otherwise, the unit cell problem is solved to obtain the new thermal properties under the temperature. The GP model is updated based on the enriched database of the thermal properties.
(5) Equations (13) and (23) are iterated until convergent results of T_0 and I_0 are obtained.
(6) Finally, the T_1 and I_1 in each unit cell can be obtained by Eqs. (9), (10) and (24). The first-order approximations for T^ε and I^ε can be reconstructed by:

$$T^\varepsilon = T_0 + \varepsilon T_1 + O\left(\varepsilon^2\right), \tag{31}$$

$$I^\varepsilon = I_0 + \varepsilon I_1 + O\left(\varepsilon^2\right). \tag{32}$$

In this work, the Cartesian meshes are used. The finite volume method and discrete ordinate method are employed to solve the heat conduction and radiative transfer equations, respectively. Details of the numerical methods can be found in Refs. [17, 30]. In addition, it should be mentioned that the value of the small parameter ε used in the computations has no influence on the final results. The reason is that the solutions of the equations in the unit cell, such as Eq. (9) and Eq. (24), are inversely proportional to the ε in the coordinate $\mathbf{y}$. Thus, the ε is cancelled out in Eqs. (31) and (32) when calculating the final results. More detailed explanations can be found in Section 3 of Ref. [17]. In this

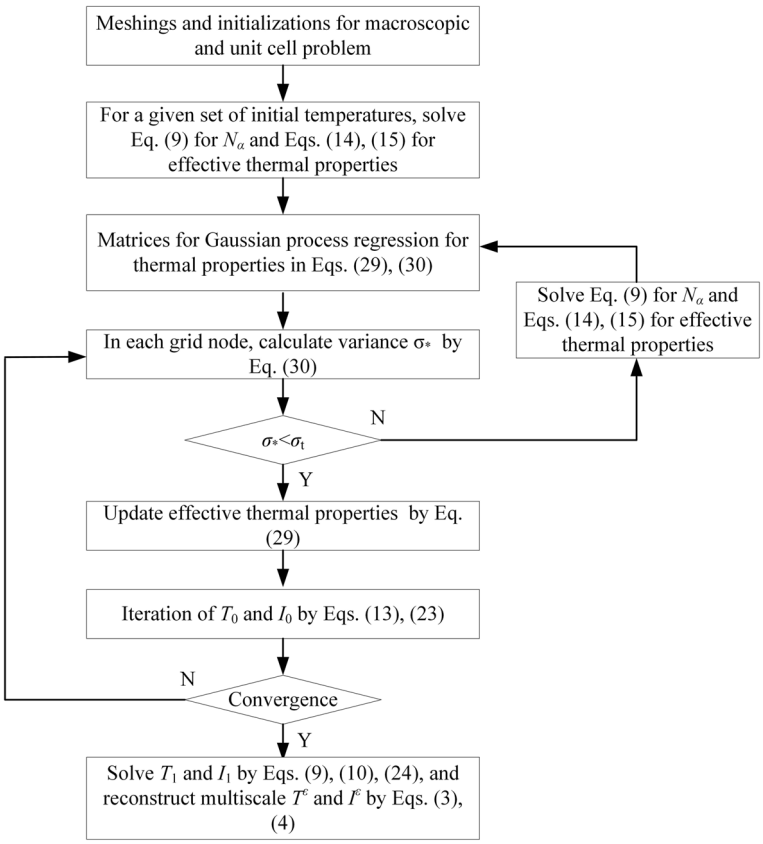

Fig. 3 Multiscale computational procedure with Gaussian process regression for conduction-radiation heat transfer problems with temperature-dependent thermal properties

work, the ε is determined as the ratio between the spatial steps in a unit cell and in the whole domain. Therefore, $\varepsilon = 1/4$ is used in Example 1 and Example 2 in the following section.

4 Numerical examples

4.1 Example 1

In this section, two-dimensional numerical examples will be used to validate the proposed multiscale method. The examples are similar to the examples in Ref. [17], which are heat transfer in SiO_2 aerogel doped with TiO_2 opacifier particles. Because the effective coefficients for radiative transfer are the simple volumetric average, the corresponding GP model is not necessary. Therefore, these coefficients are still assumed to be constant in this work. The absorption coefficients for SiO_2 aerogel and TiO_2 are 15.4 m^{-1} and 7208 m^{-1}, and the scattering coefficients are 24.8 m^{-1} and 0 m^{-1}. The following polynomials are used to calculate the thermal conductivities, which are obtained by fitting the data in Ref. [30]:

$$T_s = (T[\mathrm{K}] - 850)/360.6, \tag{33}$$

$$k_{SiO_2}[\mathrm{Wm^{-1}K^{-1}}] = 0.002179T_s^3 + 0.005754T_s^2 + 0.009287T_s + 0.02087, \tag{34}$$

$$k_{\mathrm{TiO_2}}[\mathrm{Wm^{-1}K^{-1}}] = -0.3295T_{\mathrm{s}}^3 + 0.9424T_{\mathrm{s}}^2 - 1.047T_{\mathrm{s}} + 3.745. \tag{35}$$

The range of the temperature T in Eq. (33) for the correlations in Eqs. (34) and (35) is 300 K ~ 1400 K.

The first example is a 1 mm × 0.1 mm region with ten 0.1 mm × 0.1 mm unit cells [17], as shown in Fig. 4. The TiO_2 particle is assumed to be a circle with a diameter of 20 μm. The temperature T_{h} on the left boundary is 900 K, 1100 K or 1300 K. The temperature T_{c} on the right boundary is specified as 400 K. The boundaries are assumed to be black boundaries for the radiation. Periodic boundary conditions are used on the other boundaries. For the fully-resolved simulations, the size of the mesh for a unit cell is 400 × 400 and that for the whole domain is 4000 × 400. The grid independence for effective thermal conductivities can be found in Ref. [17]. As for the homogenized equations, the grid size is 1000 × 100.

The criterion for convergence is that the relative error between two iterations is less than 10^{-8}. Because the grid size is relatively large and the thermal conductivities are temperature-dependent, the convergence for fully-resolved simulation is slow. Therefore, in this work, the temperature results of the macroscopic homogenized equations are used as the initial temperatures for the fully-resolved simulations to speed up the convergence. The relative errors of the temperature and radiative intensity fields of the multiscale simulations are defined as:

$$E_T = \sqrt{\sum_{i,j}\left(T_{i,j}^{\mathrm{M}} - T_{i,j}^{\mathrm{F}}\right)^2 / \sum_{i,j}\left(T_{i,j}^{\mathrm{F}} - T_{\mathrm{ref}}\right)^2}, E_I = \sqrt{\sum_{i,j,k}\left(I_{i,j,k}^{\mathrm{M}} - I_{i,j,k}^{\mathrm{F}}\right)^2 / \sum_{i,j,k}\left(I_{i,j,k}^{\mathrm{F}} - I_{\mathrm{ref}}\right)^2}, \tag{36}$$

where the subscripts i and j are the indices for 2D grid nodes and k is the index for discrete directions of radiative intensities. The superscripts M and F represent the results of the multiscale simulations and the fully-resolved simulations. The reference temperature is the average of the two boundary temperatures: $T_{\mathrm{ref}} = (T_{\mathrm{h}} + T_{\mathrm{c}})/2$, and the reference radiative intensity is $I_{\mathrm{ref}} = \sigma_{\mathrm{B}} T_{\mathrm{ref}}^4/\pi$.

Taking the problem with 1300 K left boundary temperature as an example, the unit cell problem is firstly solved under 6 temperatures: 400 K, 600 K, 800 K, 1000 K, 1200 K and 1300 K. An initial GP model for the effective thermal conductivities is established according to the data on the 6 temperatures. When the σ_* of the GP model on a new temperature is larger than the threshold σ_{t}, the unit cell problem is solved, the data set is updated and a new GP model is built. The influence of the value of σ_{t} is considered by setting σ_{t} as 10^{-2} to 10^{-6}. The results for the multiscale simulations are given in Table 2. Evidently, when σ_{t} decreases, the number of temperature points on which the effective thermal conductivity is calculated increases. The CPU time increases because more unit

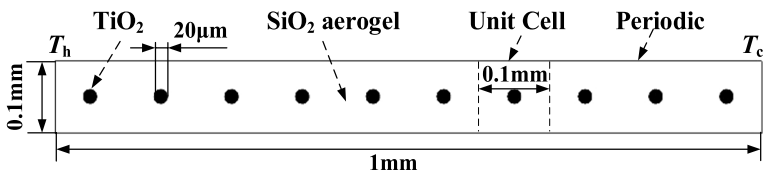

Fig. 4 Computational domain for Example 1

Table 2 Results for the multiscale simulations with different threshold σ_t

σ_t	Number of data points for GP model	CPU time	Relative error of T_0	Relative error of T^ϵ
10^{-2}	6	4.20 h	1.356%	1.104%
10^{-3}	8	4.84 h	1.290%	1.020%
10^{-4}	11	6.64 h	1.274%	1.000%
10^{-5}	14	8.51 h	1.274%	1.000%
10^{-6}	24	11.47 h	1.274%	1.000%

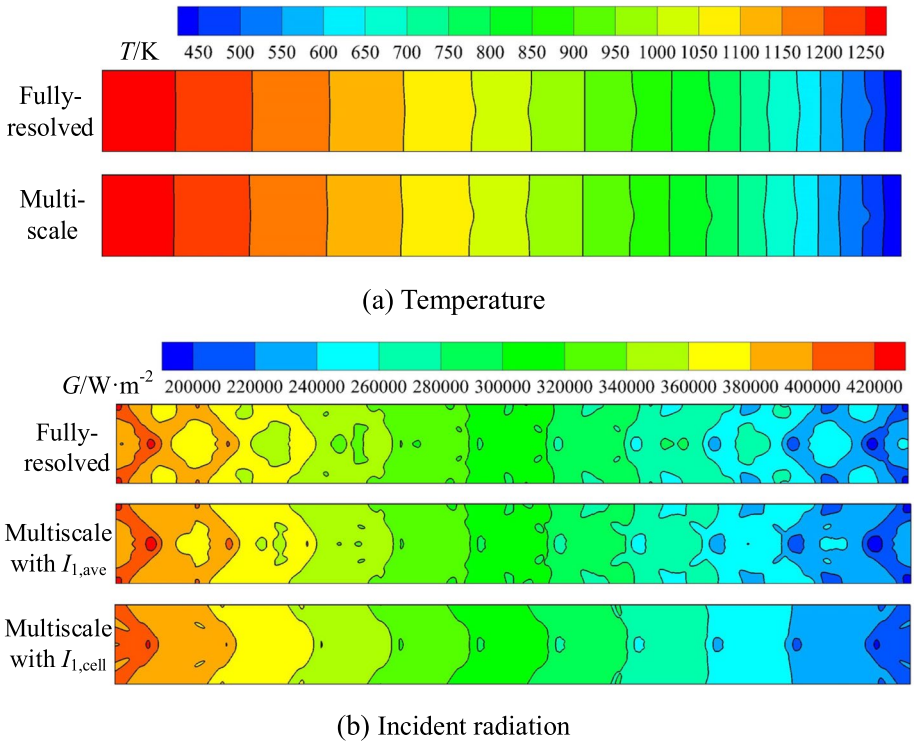

Fig. 5 The temperature and incident radiation fields of the fully-resolved simulation and the multiscale simulation

cell calculations are conducted and the dimension of the matrices in Eqs. (29) and (30) increases. As a comparison, the CPU time for the fully-resolved simulation is 69.2 h, although the solution of the homogenized equation is used as the initial temperature. Thus, the multiscale method increases the efficiency of the simulations. Meanwhile, it can be found that $\sigma_t = 10^{-4}$ is sufficient for the simulation because a smaller threshold cannot further increase the accuracy. Therefore, a proper threshold can be chosen to guarantee both the accuracy and efficiency of the multiscale model, and $\sigma_t = 10^{-4}$ is used in the rest of the work.

The temperature and incident radiation fields of the fully-resolved simulation and the multiscale simulation with $\sigma_t = 10^{-4}$ are shown in Fig. 5. The incident radiation in Fig. 5 is defined as $G = \sum_k w_k I_k$, where w_k and I_k are the weights and discrete radiative intensities in the discrete ordinate method. Both the $I_{1,\text{cell}}$ in Eq. (26) and the $I_{1,\text{ave}}$ in Eq. (27)

Table 3 Results of the multiscale simulations with different boundary temperature T_h (FR represents fully-resolved)

T_h	CPU time	CPU time of FR simulation	Relative error of T_0	Relative error of T^ϵ	Relative error of I_0	Relative error of I^ϵ with $I_{1,cell}$	Relative error of I^ϵ with $I_{1,ave}$
900 K	4.99 h	23.3 h	0.796%	0.305%	13.72%	11.84%	6.54%
1100 K	5.39 h	66.4 h	1.081%	0.773%	13.06%	11.25%	6.21%
1300 K	6.64 h	69.2 h	1.274%	1.000%	12.47%	10.72%	5.90%

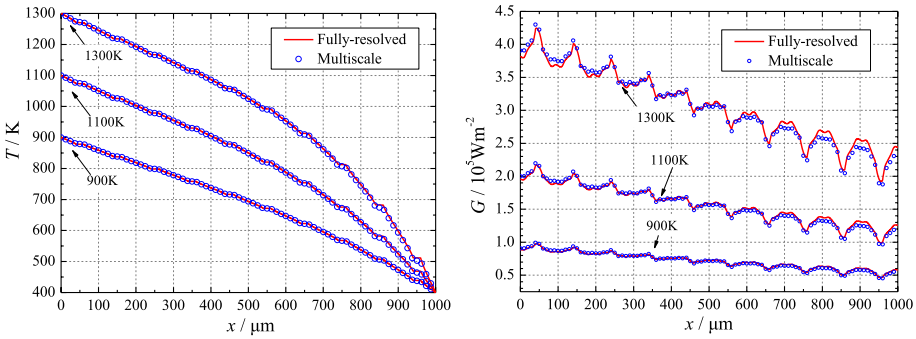

(a) temperature (b) incident radiation

Fig. 6 The temperature and incident radiation profiles of the fully-resolved simulations and the multiscale simulations on line $y = 0.05$ mm

are used to reconstruct the radiative intensity fields. It can be seen that the temperature and incident radiation fields of both the simulations coincide well with each other. The multiscale model can provide detailed small scale fluctuations of temperature and radiative intensity fields. The relative errors of the incident radiation are 12.47% for I_0, 10.72% for I^ϵ with $I_{1,cell}$, and 5.90% for I^ϵ with $I_{1,ave}$. Fig. 5 (b) also demonstrates that the $I_{1,cell}$ underpredicts the fluctuations and $I_{1,ave}$ provides a better result.

The 900 K and 1100 K are also used as the left temperature boundary conditions to show the influence of macroscopic temperature gradient on the multiscale simulations. The errors of temperature and radiative intensity are given in Table 3. The results demonstrate that the multiscale model can provide accurate results of the coupled conduction-radiation heat transfer in composites. The temperature and incident radiation profiles along horizontal line $y = 0.05$ mm are also shown in Fig. 6. It can be seen that the fluctuations of temperature and radiation induced by the particle are reproduced by the multiscale model.

Finally, the influence of radiation on the accuracy of the multiscale method is considered. The 1300 K and 400 K are used as the temperature boundary conditions. The grid size is still 4000×400. The absorption and scattering coefficients are multiplied by a factor to tune the effects of radiation. The relative errors of temperature and radiative intensity fields for different multipliers are given in Table 4. Although the influence on the error of temperature is insignificant, the error of radiation intensity increases with the increase of absorption and scattering coefficients. The reason can be found in Fig. 7 and Fig. 8, where the profiles of incident radiations with different multipliers are presented. The $\alpha_2 = 72080$ m^{-1} corresponds to the multiplier 10 in Fig. 8. The profiles have similar

Table 4 Results of the multiscale simulations with different multipliers of the absorption and scattering coefficients

Multiplier	Relative error of T_0	Relative error of T^{ϵ}	Relative error of I_0	Relative error of I^{ϵ} with $I_{1,ave}$
0.01	1.682%	1.525%	0.222%	0.093%
0.1	1.712%	1.554%	2.055%	0.805%
1	1.274%	1.000%	12.47%	5.90%
2	1.064%	0.675%	18.31%	11.32%
5	1.199%	0.844%	25.78%	20.15%
10	1.541%	1.286%	30.39%	28.45%

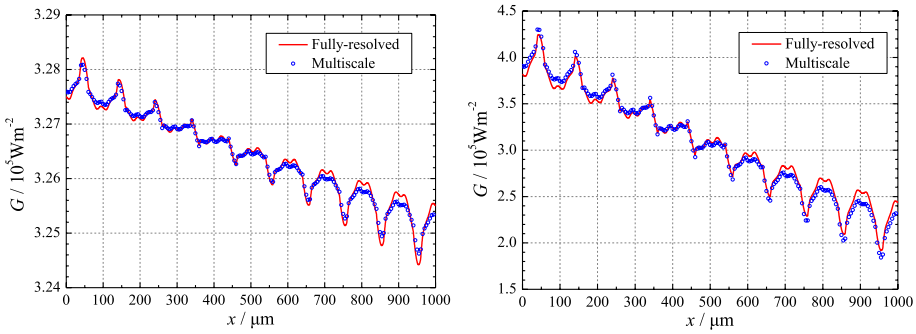

Fig. 7 The incident radiation profiles of the fully-resolved simulations and the multiscale simulations on line $y = 0.05$ mm with different multipliers of the absorption and scattering coefficients

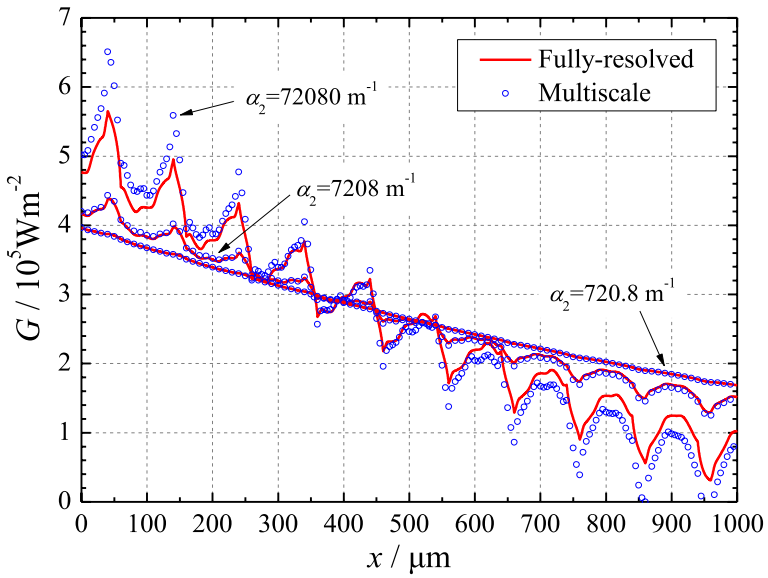

Fig. 8 The incident radiation profiles of the fully-resolved simulations and the multiscal simulations on line $y = 0.05$ mm with different absorption coefficients a_2

fluctuations due to the particles, but the magnitudes of the fluctuations and variations of the radiation are different. When the coefficients are small, the interaction between heat and radiation transfer is weak. The fluctuations and variations of the radiation are small

Table 5 Results of the multiscale simulations with different absorption coefficients

α_1 /m^{-1}	α_2 /m^{-1}	β_1 /m^{-1}	β_2 /m^{-1}	Relative error of T_0	Relative error of T^ε	Relative error of I_0	Relative error of I^ε with $I_{1,\text{ave}}$
154	72,080	248	0	1.541%	1.286%	30.39%	28.45%
154	7208	248	0	1.818%	1.635%	7.439%	3.115%
154	720.8	248	0	1.993%	1.844%	0.066%	0.041%

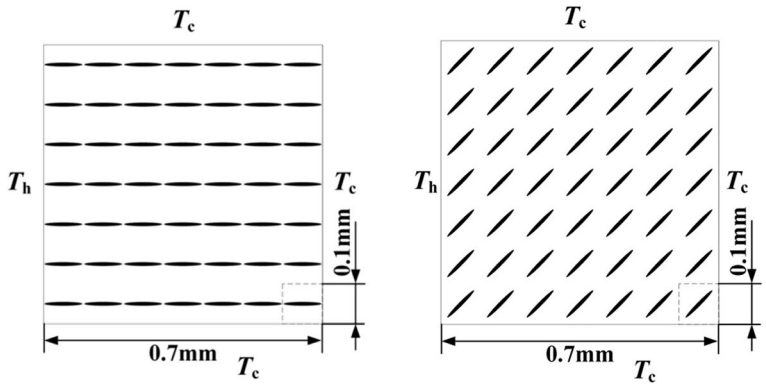

(a) Horizontally aligned particle (b) Tilted particle

Fig. 9 Computational domains for Example 2

and the relative errors of the radiation are also small. On the contrary, large coefficients lead to large fluctuations and variations of the radiation and therefore large errors. Furthermore, for the coefficients with multiplier 10, different absorption coefficients α_2 for the particles are used and the results are compared in Table 5 and Fig. 8. It can be seen that the errors of the radiation decrease as the values of the absorption coefficients of the two components become closer and the fluctuations become weaker.

4.2 Example 2

In this section, the coupled conduction and radiation heat transfer with anisotropic structures are simulated [17]. The structures are shown in Fig. 9, which are composed of 7×7 unit cells. The size of the unit cell is 0.1 mm and the size of the domain is 0.7 mm. The lengths of the major and minor axes of the elliptical particles are 94.9 μm and 9.49 μm. The particles are horizontally aligned or 45° tilted. The properties of the materials are the same as in Example 1. The temperature on the left boundary is specified as $T_h = 1300$ K and the temperature on the other boundaries is $T_c = 400$ K. The grid size of a unit cell is 400×400, and that of the fully-resolved simulation is 2800×2800. The grid size of the macroscopic homogenized simulation is 700×700.

The temperature and incident radiation fields for both the fully-resolved simulations and the multiscale simulations are given in Fig. 10 and Fig. 11. It can be seen that the multiscale results can reproduce the local temperature and radiation fluctuations due to the elliptical particles (Table 6). In addition, the CPU times of the fully-resolved simulations are 596.1 h and 500.2 h for the horizontally aligned and tilted particles, respectively. The CPU times of the multiscale simulations are 11.7 h and 13.7 h.

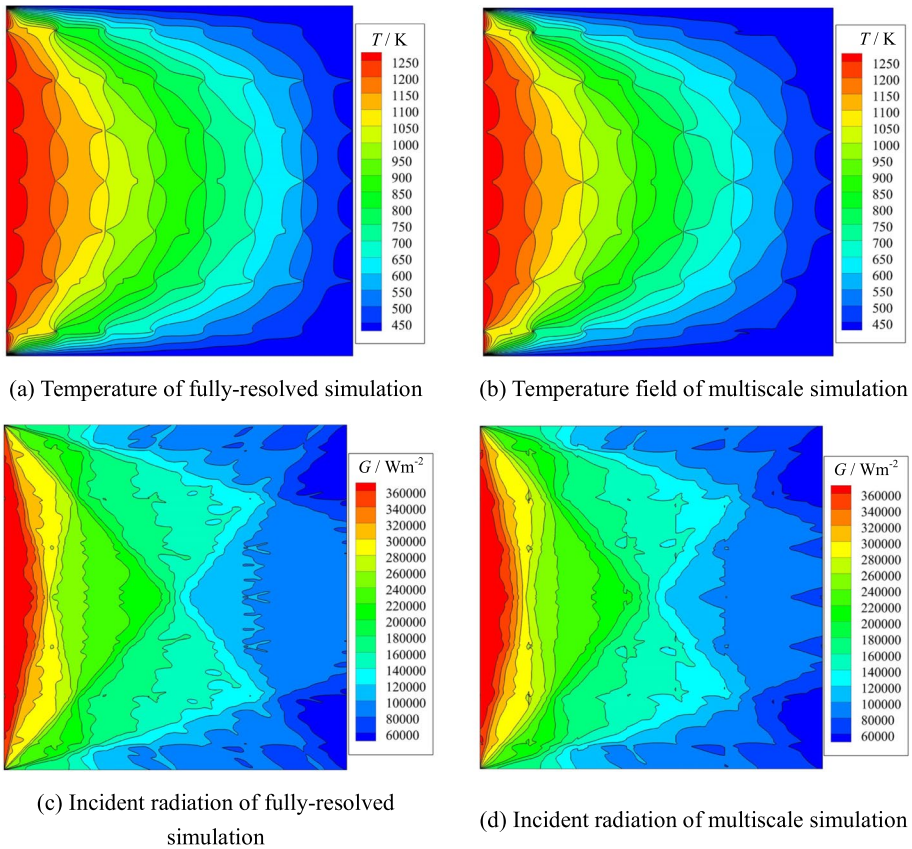

(a) Temperature of fully-resolved simulation

(b) Temperature field of multiscale simulation

(c) Incident radiation of fully-resolved simulation

(d) Incident radiation of multiscale simulation

Fig. 10 Temperature and incident radiation fields for horizontally aligned particles

5 Conclusions

In the above research, the homogenization of the coupled conduction and radiative transfer equations with temperature-dependent thermal properties has been conducted. The Taylor expansions of the thermal properties about the average temperature are used in the analysis. Both the homogenized equations and the unit cell problems are derived. It is proved that the macroscopic average temperature can be used in the unit cell problems to determine the effective thermal properties. The homogenized equations for T_0, I_0 and the equations for T_1, I_1 are the same as the equations in the analysis with constant thermal properties. The effect of the temperature-dependent thermal properties only occurs in the higher-order corrections such as the equation for T_2.

Based on the homogenization analysis, the multiscale numerical method has been proposed. The cell problem is solved to provide effective thermal properties for the macroscale iterations. In order to prevent the repetitive calculation of the cell problem, the GP regression is introduced to build a correlation between the effective thermal properties and the temperature. The GP model is updated during the iteration according to the variance of the model.

By comparing with the results of fully-resolved simulations of conduction-radiation heat transfer in composite with isotropic and anisotropic periodic structures, the proposed multiscale method is validated. By using a proper variance threshold for the GP

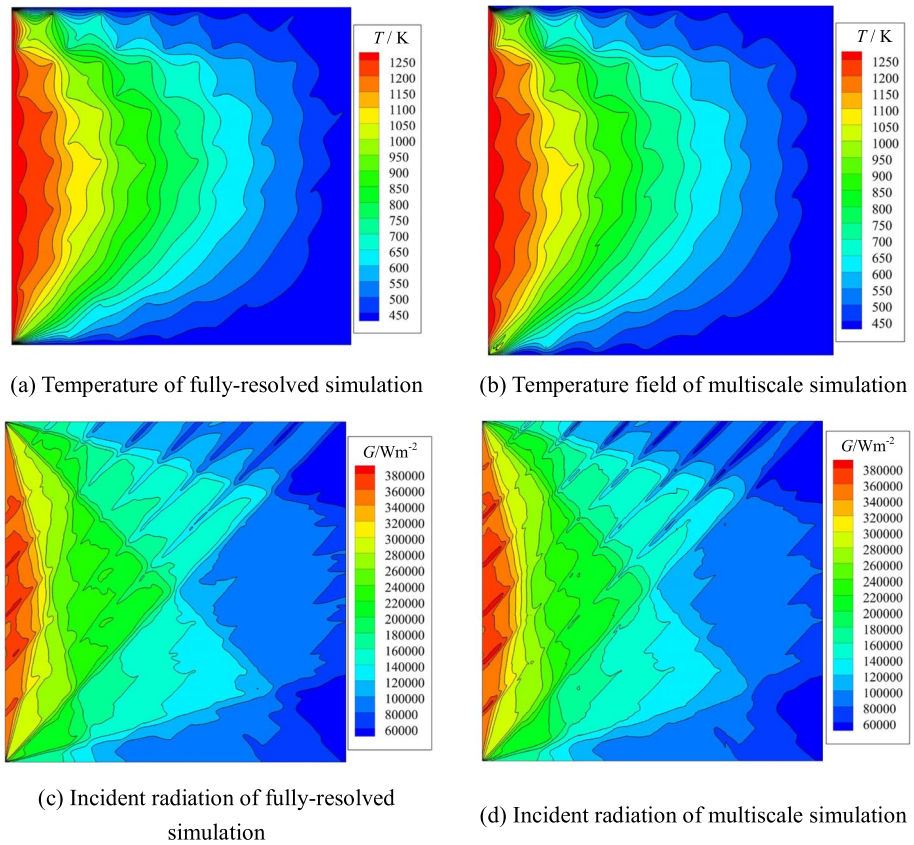

(a) Temperature of fully-resolved simulation

(b) Temperature field of multiscale simulation

(c) Incident radiation of fully-resolved simulation

(d) Incident radiation of multiscale simulation

Fig. 11 Temperature and incident radiation fields for tilted particles

Table 6 Errors of the multiscale simulations for Example 2

Structure	Relative error of T_0	Relative error of T^{ϵ}	Relative error of I_0	Relative error of I^{ϵ} with $I_{1,\text{cell}}$	Relative error of I^{ϵ} with $I_{1,\text{ave}}$
Horizontally aligned particle	11.27%	9.84%	8.83%	7.86%	5.27%
Tilted particle	7.92%	5.10%	13.22%	11.73%	10.24%

model, the accuracy and efficiency of the multiscale method can be guaranteed. The multiscale method can provide both the average temperature and radiative intensity fields and their fluctuations due to the local structures. It is found that the $I_{1,\text{ave}}$ can provide better correction of the radiative intensity, which is the average of the $I_{1,\text{all}}$ solved in the whole domain and the $I_{1,\text{cell}}$ solved in the individual cell with zero boundary incoming. It is also found that the error of the radiation increases with the magnitude of the absorption and scattering coefficients and the difference between the coefficients of different components. The proposed multiscale model can be used in further studies on the high-temperature heat transfer in composite materials with periodic structures. It should be mentioned that the analysis in this work is for the interior of composites. The

boundary layer problems should be studied in the future for the correction of boundary conditions. More detailed analysis of the homogenization of the radiative transfer equation is also needed to obtain a clearer boundary condition for I_1 [31, 32].

Acknowledgements
Not applicable.

Author contributions
All the authors contributed to this manuscript. All authors read and approved the final manuscript.

Funding
This study is supported by the National Numerical Windtunnel Project of China (NNW2018ZT2-A04, NNW2020ZT3-A22) and the National Natural Science Foundation of China (No. 51906186).

Availability of data and materials
The datasets used and/or analyzed during the current study are available from the corresponding author on reasonable request.

Declarations

Competing interests
The authors declare that they have no competing interests.

Received: 22 June 2022 Accepted: 14 August 2022
Published online: 14 September 2022

References

1. Nguyen ST, Tran-Le AD, Vu MN, To QD, Douzane O, Langlet T (2016) Modeling thermal conductivity of hemp insulation material: A multi-scale homogenization approach. Build Environ 107:127–134
2. Peng X, Zhong Y, Wang P, Luo D (2019) Estimation of thermal conduction in hollow-glass-beads-filled cement-based composites by variational asymptotic homogenization method. Appl Therm Eng 161:114191
3. He YL, Xie T (2015) Advances of thermal conductivity models of nanoscale silica aerogel insulation material. Appl Therm Eng 81:28–50
4. Bensoussan A, Lions JL, Papanicolaou G (1978) Asymptotic analysis for periodic structures, 1st edn. North-Holland, Amsterdam
5. Cioranescu D, Donato P (1999) An introduction to homogenization. Oxford University Press, Oxford
6. Kamiński M (2003) Homogenization of transient heat transfer problems for some composite materials. Int J Eng Sci 41(1):1–29
7. Matine A, Boyard N, Legrain G, Jarny Y, Cartraud P (2015) Transient heat conduction within periodic heterogeneous media: A space-time homogenization approach. Int J Therm Sci 92:217–229
8. Bennai F, Abahri K, Belarbi R, Tahakourt A (2016) Periodic homogenization for heat, air, and moisture transfer of porous building materials. Numer Heat Tr B-Fund 70(5):420–440
9. Allaire G, El Ganaoui K (2009) Homogenization of a conductive and radiative heat transfer problem. Multiscale Model Simul 7(3):1148–1170
10. Allaire G, Habibi Z (2013) Homogenization of a conductive, convective, and radiative heat transfer problem in a heterogeneous domain. SIAM J Math Anal 45(3):1136–1178
11. Asakuma Y, Kanazawa Y, Yamamoto T (2014) Thermal radiation analysis of packed bed by a homogenization method. Int J Heat Mass Transf 73:97–102
12. Yang Z, Cui J, Ma Q (2014) The second-order two-scale computation for integrated heat transfer problem with conduction, convection and radiation in periodic porous materials. Discrete Continuous Dyn Syst Ser B 19(3):827–848
13. Yang Z, Cui J, Sun Y, Ge J (2015) Multiscale computation for transient heat conduction problem with radiation boundary condition in porous materials. Finite Elem Anal Des 102–103:7–18
14. Yang Z, Sun Y, Cui J, Yang Z, Guan T (2018) A three-scale homogenization algorithm for coupled conduction-radiation problems in porous materials with multiple configurations. Int J Heat Mass Transf 125:1196–1211
15. Haymes R, Gal E (2018) Iterative multiscale approach for heat conduction with radiation problem in porous materials. ASME J Heat Transf 140(8):082002
16. Huang J, Cao L (2014) Global regularity and multiscale approach for thermal radiation heat transfer. Multiscale Model Simul 12(2):694–724
17. Tong ZX, Li MJ, Yu YS, Guo JY (2021) A multiscale method for coupled steady-state heat conduction and radiative transfer equations in composite materials. ASME J Heat Transf 143(8):082102
18. Muliana AH, Kim JS (2010) A two-scale homogenization framework for nonlinear effective thermal conductivity of laminated composites. Acta Mech 212(3):319–347
19. Chung PW, Tamma KK, Namburu RR (2001) Homogenization of temperature-dependent thermal conductivity in composite materials. J Thermophys Heat Transf 15(1):10–17
20. Zhai H, Wu Q, Yoshikawa N, Xiong K, Chen C (2021) Space-time asymptotic expansion method for transient thermal conduction in the periodic composite with temperature-dependent thermal properties. Comput Mater Sci 194:110470

21. Fish J (2013) Practical multiscaling. Wiley, Chichester
22. Monteiro E, Yvonnet J, He QC (2008) Computational homogenization for nonlinear conduction in heterogeneous materials using model reduction. Comput Mater Sci 42(4):704–712
23. Weinan E (2011) Principles of multiscale modeling. Cambridge University Press, Cambridge
24. Tong ZX, He YL, Tao WQ (2019) A review of current progress in multiscale simulations for fluid flow and heat transfer problems: The frameworks, coupling techniques and future perspectives. Int J Heat Mass Transf 137:1263–1289
25. Asproulis N, Drikakis D (2013) An artificial neural network-based multiscale method for hybrid atomistic-continuum simulations. Microfluid Nanofluid 15(4):559–574
26. Roehm D, Pavel RS, Barros K, Rouet-Leduc B, McPherson AL, Germann TC, Junghans C (2015) Distributed database kriging for adaptive sampling (D^2KAS). Comput Phys Commun 192:138–147
27. Stephenson D, Kermode JR, Lockerby DA (2018) Accelerating multiscale modelling of fluids with on-the-fly Gaussian process regression. Microfluid Nanofluid 22(12):139
28. Rasmussen CE, Williams CKI (2006) Gaussian processes for machine learning. MIT Press, Cambridge
29. Howell JR, Siegel R, Mengüç MP (2010) Thermal radiation heat transfer, 5th edn. CRC Press, Boca Raton
30. Xie T, He YL (2016) Heat transfer characteristics of silica aerogel composite materials: Structure reconstruction and numerical modeling. Int J Heat Mass Transf 95:621–635
31. Bensoussan A, Lions PL, Papanicolaou GC (1979) Boundary layers and homogenizatlon of transport processes. Publ Res Inst Math Sci 15:53–157
32. Dumas L, Golse F (2000) Homogenization of transport equations. SIAM J Appl Math 60(4):1447–1470

Publisher's Note